A novel magnetic resonance imaging probe specifically targeting vascular endothelial growth factor receptor 2: synthesis, characterization, and biological evaluation

Xiaoguang You[a,b] and Yikai Xu[*,a]

[a]Department of Radiology, The Affiliated Hospital of Southern Medical University, Nanfang Hospital, No. 1838, Guangzhou Ave, Guangzhou, China

[b]Department of Radiology, The Affiliated Hospital of Hainan Medical University, No. 31, Longhua Road, Haikou,China

[*]Corresponding author: Yikai Xu, Department of Radiology, The Affiliated Hospital of Southern Medical University, Nanfang Hospital, No. 1838, Guangzhou Ave, Guangzhou, China

Telephone: +86 020-61642083; Email address: xyknfyy@126.com

Abstract: Vascular endothelial growth factor (VEGF) is strongly expressed in most tumors and promotes both tumor growth and vascularization. The peptide, $VEGF_{125-136}$, consisting of 12 amino acids is encoded by exon 6 of the *VEGF* gene and inhibits VEGF activity by blocking the binding of VEGF to the VEGFR2 receptor. The aim of the present study was to develop a targeting probe for magnetic resonance imaging (MRI) of tumors by conjugating $VEGF_{125-136}$ to gadolinium (III) (Gd(III)) (VGd) through the formation of chelates. The targeting efficiency of VGd to human hepatocellular carcinoma (HCC) cell line, BEL-7402, was subsequently determined both in *vitro* and in *vivo*. In the in *vitro* studies, the MRI results of BEL-7402 cells treated with VGd showed a significantly higher T1 signal-to-noise ratio than that of both the competitive group, namely, those treated with VGd and $VEGF_{125-136}$ and the control group, a scramble peptide conjugated to Gd(III) (SGd). In *vivo*, when xenografts of BEL-7402 cells were established in mice and then VGd or SGd were injected via tail vein, MRI showed that the tumor signal from VGd initially decreased from 5 min to 120 min and then it increased at 120 min post injection. The peak signal was observed at 120 min after the injection. In contrast, no distinct peak was observed for SGd. Undoubtedly, these findings indicate that VGd can target VEGFR2, highly expressed by BEL-7402 cells, enabling targeting MRI with high efficacy to be achieved both in *vitro* and in *vivo*.

Keywords:

$VEGF_{125-136}$; peptide; gadolinium; MRI; liver cancer xenograft

INTRODUCTION

Cancer is one of the most serious diseases that threaten human beings, and an early diagnosis of tumors, particularly for small ones, is of great importance for improving patient prognosis. Thus, an important task for molecular imaging is to generate accurate images that can facilitate the early diagnosis of cancers.[1] Most of the tumor-imaging agents currently used for MRI in the clinic are gadolinium Gd- or iron-based contrast agents, which generally image soft tissues with high spatial resolution and are effective for noninvasive imaging of physiological properties, such as diffusion, vascularity, and perfusion of the tissues of interest. However, the shortcoming of these agents limiting their broad application is the low sensitivity. The modification with targeting ligands, such as antibodies, proteins, and peptides, even though improved the probe delivery, it could not deliver a sufficient amount of agents to detect the target tissues.[2, 3] Thereby, nanoparticles have been used to load large amount of probes for increasing the local concentration of contrast agents.[2-4] The major limitation of nanoparticle-based MRI contrast agents is that they possess huger size than the renal filtration threshold (~4.5 nm), and cannot be readily excreted from the body, resulting in toxic side effects, for example, systemic nephrogenic fibrosis, particularly in case of long-term tissue retention of high-dose Gd(III)-based MRI agents.[5-9]

The challenges in MRI for molecular imaging can be overcome by the selection of molecular biomarkers and using MRI agents, which can be readily excreted from the

body. Stable Gd(III) chelates, such as DOTA, DO3A, DTPA, have been proven safe and receiving increasing attention as MRI agents.[2, 7, 10, 11] For targeted contrast agents, the sufficiently expressed biomarkers at local position play great role in molecular imaging. As previously reported, VEGF is strongly expressed in tumor tissues and its expression has been found to be proportional to the degree of malignancy for tumors.[12, 13] VEGF binds the VEGFR2 receptor which is also strongly expressed in most tumor cells, as well as in endothelial cells that mediate tumor neovascularization.[14, 15] Previously, $VEGF_{125\text{-}136}$, a 12-amino acid peptide encoded by exon 6 of the *VEGF* gene, was found to block the specific binding of VEGF to the VEGFR2 receptor.[16] Based on these findings, we hypothesized that targeted in *vivo* tumor imaging may be achieved with the use of Gd(III)-based contrast agents labeled with the $VEGF_{125\text{-}136}$ peptide as depicted in Scheme 1. Furthermore, the use of VGd as a contrast agent would provide a more widely applicable agent based on the strong expression profile of VEGF in many tumors. Therefore, in our present study, $VEGF_{125\text{-}136}$ will be conjugated to Gd(III) through the formation of chelates and its ability to target VEGFR2 in BEL-7402 liver carcinoma cells both in *vitro* and in *vivo* will be investigated. Our study might develop a promising Gd(III)-based targeted MRI agent with high imaging efficacy for potential clinical use.

MATERIALS AND METHODS

Materials

All chemicals and solvents were used without further purification unless otherwise stated. The Fmoc-protected $VEGF_{125\text{-}136}$ peptide (QKRKRKKSRYKS) resin and its

scrambled peptide (QKYSKQKKSSQKQK) resin were purchased from GL Biochem Ltd (China). 2-(1H-benzotriazol-1-yl)-1,1,3,3-tetramethyluronium hexafluorophosphate (HBTU), hydroxybenzotriazole (HOBt), and N,N-diisopropylethylamine (DIPEA) was purchased from Aladdin. Gadolinium acetic acid was purchased from Strem Chemicals (USA). Piperidine was purchased from Guangzhou Chemical Reagent Factory. DOTA-Tris (t-Bu ester) was purchased from TCL (Tokyo, Japan). Gadolinium acetic acid was obtained from Shanghai Di Bai Chemial Technology Co., Ltd.

General method of characterization

Matrix-assisted laser desorption/ionization time-of-flight (MALDI-TOF) mass spectra were recorded on a Bruker Autoflex III MALDI-TOF MS in a linear mode. T1 relaxation constants were measured with a 3.0T MRI scanner (GE, Pittsburgh, PA, USA) at 37 ℃ in distilled water. The Gd concentration in VGd or SGd was determined with an inductively coupled plasma mass spectrometer (ICP-MS, Thermo Fisher, USA).

Synthesis of Gd(III) chelates

The 12-amino acid $VEGF_{125-136}$ peptide (1.1 g) and the scrambled peptide (1.1 g) were deprotected with 15 ml piperidine/DMF solution (1:4, v/v) in solid phase peptide synthesis tubes to remove the Fmoc protecting groups. After washed with DMF (×3) and DCM (×3), DOTA-Tris (t-Bu ester) (290 mg, 0.5 mmol), HBTU (379 mg, 1 mmol), HOBt (100 mg), and DIPEA (500 μl) were added to each tube. The reaction continued under shaking at room temperature for 2 h. Then the resins were washed

with DMF (×3) and DCM (×3) before cleavage with a mixture of trifluoroacetic acid/triisobutylsilane/water (96.5:1.0:2.5, v/v/v) for 5 h. The products were subsequently precipitated with cold diethyl ether twice and dried under reduced pressure at room temperature to yield $VEGF_{125-136}$-DOTA or scramble-DOTA. MALDI-TOF ($VEGF_{125-136}$-DOTA) (*m*/*z*, $[M]^+$): 1978.36 (obsd.); 1978.15 (calcd). MALDI-TOF (scramble-DOTA) (*m*/*z*, $[M]^+$): 2109.43 (obsd.); 2109.15 (calcd).

The dried sample was further dissolved in 3 ml double-distilled water, to which gadolinium acetic acid (82 mg, 0.2 mmol) was added. During reaction, the pH was maintained at 6.5~7.0 at 50 ℃. After 24 h, the pH was adjusted to ~11 using aqueous NaOH (0.2 M) to remove most of the access Gd. Then the pH was neutralized to ~7 using HCl (0.2 M), followed by cold-drying to obtain crude white products. Further, the products was purified using high-performance liquid chromatography (HPLC), with a C18 column used for the stationary phase and acetonitrile/water applied for the mobile phase. MALDI-TOF (VGd) (*m*/*z*, $[M]^+$): 2133.79 (obsd.); 2133.06 (calcd). MALDI-TOF (SGd) (*m*/*z*, $[M]^+$): 2264.05 (obsd.); 2264.35 (calcd).

Cell culture

Human HCC cell line BEL-7402 (Chinese Academy of Medical Sciences, China) was grown in RPMI 1640 medium supplemented with 100 mL/L heat-inactivated fetal calf serum, 50,000 U/L penicillin, and 50 mg/L streptomycin. The cells were cultured under a humid condition (95%, relative humidity) at 37 ^oC containing 5% CO_2. The RPMI 1640 medium was refreshed every other day and the cells were split once the confluency was reached.

In *vitro* MRI examination

BEL-7402 cells were grown in RPMI 1640 medium in cell culture flasks (25 cm^3). When the cells reached 85% confluency, 100 μL of VGd (0.05 mmol/ml), 100 μL of SGd (0.05 mmol/ml), and 100 μL mixture of VGd and $VEGF_{125-136}$ as competitive probe test group (CPT, 0.05 mmol/ml, each) were added to flasks, respectively. Thereafter, the cells were incubated for 24 h at 37 ℃ under a humid condition at 5% CO_2. After the cells were washed with PBS (×4) and trypsinized, the cells were transferred to centrifuge tubes, followed by addition of 0.6% agarose to form a suspension. A 3.0-T MRI scanner head coil (GE, Pittsburgh, PA, USA) was used to obtain a MRI scan of each tube with the following T1 scanning parameters: repetition time (TR)/echo time (TE) = 600/15 ms, matrix = 256 × 256, thickness = 2 mm, field of view (FOV) = 20 cm, (signal-to-noise ratio = T1 mean signal/ambient noise), and region of interest (ROI) = 2 mm. The ROI was selected as the diameter for an effective T1 measuring range.

In *vivo* MR tumor imaging

Subaxillary xenografts of human BEL-7402 cells were established in 16 male nude mice (25-30 g, Slac Laboratory Animals Ltd., Shanghai, China). This animal study was approved by the independent Ethics Committee of Hainan Medical College Hospital, and all of the animals received humane care throughout the duration of the study. When the tumor diameter reached ~1.0 cm, the mice were anesthetized with pentobarbital (0.05 mg/g, i.p.) and administrated with of VGd (100 μL, 0.2 mmol

Gd/kg) and SGd (100 μL, 0.2 mmol Gd/kg) via tail vein injection. An additional 50 μL of saline was subsequently administered to flush the line and ensure that the complete dose was administered in each mouse. The mice then went through a MRI examination with a 3.0-T MRI scanner (GE) that had a dedicated mouse MRI coil (Chenguang Medical Technologies Ltd., Shanghai). Seven scans were performed on each mouse: the first scan was performed prior to the administration of contrast administration (pre-injection), while the followed scans were performed at 5, 15, 30, 60, 120, and 240 min post injection. All of the scans were conducted under the following axial fast-spin echo T1-weighted imaging conditions: TR/TE = 340/16 ms, number of excitations = 4, matrix = 128 × 128, FOV = 8 × 8 cm, slice thickness = 1.0 mm, and slice interval = 0.1. Signal intensity was obtained by averaging three measurements for three ROIs within the same slice at various time points. The diameter of each ROI was ~2.0 mm.

Immunohistological examination of VEGFR2 expression

For immunohistological staining of BEL-7402 xenografts, mice (n = 3) were injected with VGd or SGd. Then, the tumors were fixed with 4% formaldehyde, dehydrated in a gradient alcohol series and xylene, and embedded in paraffin. Sections (5 μm) were cut from each tissue block and mounted onto slides. After the sections were incubated overnight at 60 ℃, the sections were immersed in xylene (5 min×2) and then in a gradient alcohol series. After the sections were rinsed with water and 0.1 M PBS, they were immersed in methanol with 1% hydrogen peroxide at room temperature for 10

min before a final water rinse. The sections were subsequently treated with an antigen retrieval agent, rinsed with water, and blocked with non-immune horse serum. Subsequently, the sections were incubated with VEGFR2 antibody (Abcam) at 4 ℃ overnight and then washed with 0.1 M PBS, followed by incubation with an appropriate biotinylated secondary antibody (Abcam) for 20 min at 37 ℃. After rinsed with PBS, the sections were incubated with streptavidin-horseradish peroxidase at 37 ℃ for 20 min. After washed with PBS, bound antibodies were visualized with 3,3′-diaminobenzidine. A final thorough washing of the sections was followed by a counterstaining step with hematoxylin.

Biodistribution study

Tumor-bearing mice were sacrificed at 1 and 7 days post-injection. The tissues, for example, liver, lung, kidney, spleen, tumor, heart, brain, skin, femur, and muscle were collected. After dried and weighed, each sample was fully immersed in 70% nitric acid (1.0 mL). Once the sample was completely liquefied, the solution was transferred to a new centrifuge tube (15 mL) and the undissolved components were spinned down at 10,000 rpm for 20 min. Then the solution was filtrated through a syringe filter (0.22 μm, Nantong Feitebo membrane Co. Ltd, China) to further remove insoluble particles. Thereafter, the solution was diluted 10 times with deionized water and the Gd(III) concentration was detected by ICP. The average Gd(III) content in each tissue was calculated from the measured Gd(III) concentration and expressed as the percentage of injected dose per gram of organs (% ID/g).

RESULTS

The VGd and SGd in this study were purchased and used as received without further purification. After removal of the Fmoc protecting group, the free amine groups directly conjugate with DOTA-Tris (t-Bu ester) through solid-phase chemistry as shown in Figure 1. Thereafter, the products were cleaved from resins and formed chelates with gadolinium through carboxyl groups. The chemical structures of VGd and SGd were confirmed with MALDI-TOF spectra as demonstrated in Figure 2, which was also described in experimental section. The small peak appeared in the right of the major peak in Figure 2b should be ascribed to the addition of sodium element.

The plots of the T_1 and T_2 water proton relaxation values at 3.0T versus the concentration of VGd or SGd are demonstrated in Figure 3. The T1 relaxivity values (r_1) of VGd and SGd were measured to be 7.15 $mM^{-1}s^{-1}$ per Gd and 7.46 $mM^{-1}s^{-1}$ per Gd, respectively. Also, the T_2 relaxivity values (r_2) of them were determined to be 8.26 $mM^{-1}s^{-1}$ per Gd and 9.12 $mM^{-1}s^{-1}$ per Gd, respectively.

Figure 4 shows the results of the in *vitro* MRI examination of BEL-7402 cells treated with SGd, VGd and competitive group, respectively. Clearly, the samples, untreated with agents, showed extremely poor contrast. The similar result was also observed for the sample treated with SGd. Conversely, the sample treated with VGd presented significant contrast enhancement. In addition, even though the sample treated with CPT showed slightly improved contrast than the untreated groups, it was not comparable to the VGd-treated sample. Moreover, the T_1 signal-to-noise ratio (SNR) was measured accordingly at the concentrations of 0.00 and 0.05 mmol/mL as shown

in Figure 4b. Consistently, the VGd presented significantly higher SNR value than SGd and CPT groups.

To verify the targeting ability of VGd to VEGFR2 in *vivo*, it is paramount to confirm the availability of VEGFR2 in tumors. As shown in Figure 5, hematoxylin-eosin staining showed large nuclei with obvious isomerisms and visible mitotic figures and BEL-7402 tumor cell membranes positively displayed VEGFR2 for all tumor sections in the established xenografts of BEL-7402 cells. Hence, the tumors for VGd and SGd treatment in this study possessed the identical immunohistochemical conditions.

Further, the MRI scanning of tumor-bearing mice was performed to investigate the imaging effects of SGd and VGd as shown in Figure 6. The scanning time points were set at 5, 15, 30, 60, 120, and 240 min, respectively. Apparently, the images recorded from both agents reached the brightest point at 5 min and showed contrast decrease with time. However, compared with SGd, the VGd group presented relatively higher contrast enhancement at the same time point after 5 min and, moreover, it showed much slower contrast decrease. Interestingly, it showed great contrast enhancement at 120 min. Subsequently, the SNR values corresponding to the images were measured and plotted as depicted in Figure 6b, showing the consistent results.

To evaluate the retention of the contrast agents in the major organs, the biodistribution study was carried out at day 1 and day 7 post-injection in the tumor-bearing mice. The major organs were dissolved in high purity nitric acid and the Gd(III) content was measured by ICP. Figure 7 showed the biodistribution of SGd or VGd in the major organs, including muscle, femur, tumor, skin, spleen, liver, kidney, lung, heart, and

brain at day 1 and day 7 post-injection at a dose of 0.2 mmol-Gd/kg. The retention of SGd and VGd was comparable in the normal tissues and was significantly different ($p<0.01$) in the tumor at day 1 post-injection. At day 7, the retention of VGd in tumor was still significantly higher than SGd ($p<0.05$).

DISCUSSION

Development of targeted MRI molecular probes is of great importance in molecular imaging since it has the potential to improve tumor visualization and positioning accuracy. Generally, the imaging component of probes includes iron- or gadolinium-based contrast agents, while the targeting ligands popularly studied are antibodies, peptides, and aptamers. Peptides are particularly advantageous because of their low molecular weight, ease of transportation and storage, great stability, and ease of modification.[17, 18] For example, recent studies have demonstrated that the use of $\alpha_v\beta_3$ integrin, aminopeptidase N, and angiopoietin could provide targeting of a tumor and its vascular endothelial cells.[19, 20]

VEGF has 7 exon sequences, and the affinity of the peptide fragments encoded by these exons for VEGFR2 varies considerably. Previous findings suggested that the affinity of $VEGF_{125\text{-}136}$ (QKRKRKKSRYKS), a 12-amino acid peptide encoded by exon 6 for VEGFR2, was greater than that of other similar peptide fragments.[16] Furthermore, binding of $VEGF_{125\text{-}136}$ to the extracellular region of VEGFR2 has no biological activity, yet this binding event can competitively prevent the ability of VEGF from promoting tumor cell growth and angiogenesis. Therefore, irreversibly

linking $VEGF_{125-136}$ with Gd via chemical bonds was expected to provide a targeted MRI imaging enhancement.

In our present study, we first synthesized VGd and SGd through a facile standard solid-phase chemistry as demonstrated in Figure 1. MALDI-TOF (Figure 2) was employed to confirm the molecular weights of VGd and SGd (2133.52 g/mol and 2264.60 g/mol, respectively), and these weights matched their theoretical molecular weights, meaning that the chemical structures shown in Figure 1 were obtained. Furthermore, the relaxivity values including r_1 and r_2 at 3.0T for both SGd and VGd were confirmed as shown in Figure 3. The results indicated that both r_1 and r_2 of SGd were slightly higher than those of VGd. Earlier study on the MRI contrasts using CREKA as targeting peptide demonstrated that its r_1 and r_2 values were also slightly lower than those of the scrambled peptide.[11] However, the essential point in this study is to demonstrate the advantageous targeting ability of VGd over SGd. Therefore, the targeting effect will be valued more than the relaxivity, not to mention the slight difference between VGd and SGd. This question was further elucidated in the in *vitro* imaging study as indicated in Figure 4. In principle, the SGd with higher r_1 value was expected to show enhanced contrast compared with VGd since MRI agents with higher relaxivity would provide equivalent contrast at a lower dose compared with lower relaxivity agents.[7, 11] However, the results suggested that the VGd with slightly lower r_1 gave significantly greater imaging enhancement than SGd at the concentration of 0.05 mmol/mL than SGd, indicating that the targeting effect from $VEGF_{125-136}$ dominated the interaction of agents with cells. To further confirm the targeting efficacy of VGd to cells, the competitive group was added and the cells showed much poorer imaging contrast than VGd, which might attribute to the competitive binding of $VEGF_{125-136}$ to VEGFR2. These imaging studies and the

quantified SNR values in Figure 4b consistently demonstrated the great targeting efficacy of VGd to tumor cells.

To ensure the existence of VEGFR2 in tumors for both VGd and SGd groups, positive immunohistochemical staining of BEL-7402 cell membranes for VEGFR2 was employed for confirmation as shown in Figure 5, indicating the same tumor condition for both VGd and SGd groups. Further, tail vein injections of VGd or SGd were conducted to evaluate the in *vivo* imaging of contrast agents. It is found that efficient accumulation of the targeted contrast agent was observed in the tumor area at 5 min, however the contrast continuously decreased faster after 5 min for SGd than VGd. Previously, the other peptides used for MRI targeting imaging, including CREKA, ZD2, and CLT1, also indicated the similar findings that agents modified with targeting peptides would provide enhanced contrast and also slower contrast decrease with scanning time.[2, 11, 21] As illustrated in Scheme 1, the VGd, once injected via tail vein, circulated in the blood vessel and conveniently bound to the VEGFR2 highly expressed in tumors, resulting in the improved tumor uptake of VGd compared with SGd. On the contrary, SGd without targeting funtion can be easily eliminated from the mouse body within short time post-injection, certainly strongly lowering its imaging efficacy. In addition, we noted that the contrast was sharply enhanced at 120 min for VGd. Previously, Gd-labeled VEGF monoclonal antibodies was injected via a caudal intravenous injection into a mouse model of a hepatocellulcar carcinoma (HCC) hepatic transplantable tumor, the contrast agent was detected at 10 min post-injection.[22] More interestingly, the highest contrast enhancement was detected at 120 min and then the signal disappeared completely within 24 h. These results are similar to those of the present study, except that the signal for the contrast reagent was maintained for a longer period than that in the present study. It is possible that the

larger molecular weight of the monoclonal VEGF antibodies in that study underwent longer circulation time.

The retention of both agents was comparable in the normal tissues and the VGd accumulation was significantly higher in the tumor post-injection as shown in Figure 7. The targeted contrast agent displayed higher tumor uptake than the non-targeted contrast agent. The injected agents were, mostly, eliminated from the mouse within short period. The kidneys and liver, the major organ involved in the excretion of contrast agents, had a Gd(III) retention of the injected VGd or SGd per gram of tissue, higher than other organs and tissues.[11] At day 7, the Gd(III) retention was remakablly decreased in the kidneys and liver. No detectable Gd(III) was observed in the bone, muscle or brain for SGd or VGd, indicating that our contrast agent should have great safety for potential clinical use. As compared with previously reported dendrimer-based targeted Gd(III) chelates, the peptide targeted low molecular weight contrast agent, VGd, has much lower Gd(III) retention in *vivo*.

Summary

An amide linkage was used to conjugate $VEGF_{125-136}$ to Gd to develop a novel targeted contrast agent that has high T1 relaxivity. In BEL-7402 tumor cells, $VEGF_{125-136}$-Gd was found to effectively target VEGFR2 both *in vitro* and *in vivo*, and thus, this agent may be useful for targeted MRI imaging.

Acknowledgments

We would like to thank Zheng-Rong Lu (Department of Biomedical Engineering,

Case Western Reserve University, Cleveland, OH) for his guidance in the probe construction efforts. This study was funded by the National Natural Science Foundation of China (Grant no. 81160177, 81641067 and 81460262) and the Natural Science Foundation of Hainan, China (Grant no. 20158290).

Conflict of Interest

The authors declare no conflict of interest.

References

1. Li, C., Chen, T., Ocsoy, I., Zhu, G., Yasun, E., You, M., Wu, C., Zheng, J., Song, E., Huang, C. Z. and Tan, W., Gold-Coated Fe3O4 Nanoroses with Five Unique Functions for Cancer Cell Targeting, Imaging, and Therapy. *Advanced Functional Materials*, 2014, **24**, 1772-1780.

2. Tan, M., Ye, Z., Lindner, D., Brady-Kalnay, S. M. and Lu, Z. R., Synthesis and evaluation of a targeted nanoglobular dual-modal imaging agent for MR imaging and image-guided surgery of prostate cancer. *Pharm. Res.*, 2014, **31**, 1469-1476.

3. Li, J., Huang, S., Shao, K., Liu, Y., An, S., Kuang, Y., Guo, Y., Ma, H., Wang, X. and Jiang, C., A choline derivate-modified nanoprobe for glioma diagnosis using MRI. *Scientific Reports*, 2013, **3**, 1623.

4. Kuo, T., Lai, W., Li, C., Wun, Y., Chang, H., Chen, J., Yang, P. and Chen, C., AS1411 aptamer-conjugated Gd2O3:Eu nanoparticles for target-specific computed tomography/magnetic resonance/fluorescence molecular imaging. *Nano Research*, 2014, **7**, 658-669.

5. Curtet, C., Maton, F., Havet, T., Slinkin, M., Mishra, A., Chatal, J. F. and Muller, R. N., Polylysine-Gd-DTPAn and polylysine-Gd-DOTAn coupled to anti-CEA F(ab')2 fragments as potential immunocontrast agents. Relaxometry, biodistribution, and magnetic resonance imaging in nude mice grafted with human colorectal carcinoma. *Investigative radiology*, 1998, **33**, 752-761.

6. Ke, T., Jeong, E. K., Wang, X., Feng, Y., Parker, D. L. and Lu, Z. R., RGD targeted poly(L-glutamic acid)-cystamine-(Gd-DO3A) conjugate for detecting

angiogenesis biomarker alpha(v) beta3 integrin with MRT, mapping. *Int. J. Nanomed.* 2007, **2**, 191-199.

7. Flacke, S., Fischer, S., Scott, M. J., Fuhrhop, R. J., Allen, J. S., Mclean, M., Winter, P., Sicard, G. A., Gaffney, P. J. and Wickline, S. A., Novel MRI Contrast Agent for Molecular Imaging of Fibrin Implications for Detecting Vulnerable Plaques. *Circulation* 2001, **104**, 1280-1285.

8. Amirbekian, V., Lipinski, M. J., Briley-Saebo, K. C., Amirbekian, S., Aguinaldo, J. G. S., Weinreb, D. B., Vucic, E., Frias, J. C., Hyafil, F. and Mani, V., Detecting and assessing macrophages in vivo to evaluate atherosclerosis noninvasively using molecular MRI. *Proceedings of the National Academy of Sciences of the United States of America,* 2007, **104**, 961-966.

9. Sieber, M. A., Pietsch, H., Walter, J., Haider, W., Frenzel, T. and Weinmann, H. J., A preclinical study to investigate the development of nephrogenic systemic fibrosis: a possible role for gadolinium-based contrast media. *Investigative radiology*, 2008, **43**, 65-75.

10. Tan, M. and Lu, Z. R., Integrin Targeted MR Imaging. *Theranostics* 2011, **1**, 83-101.

11. Zhou, Z., Wu, X., Kresak, A., Griswold, M. and Lu, Z.-R., Peptide targeted tripod macrocyclic Gd(III) chelates for cancer molecular MRI. *Biomaterials*, 2013, **34**, 7683-7693.

12. Wang, Y., Huang, L., Wu, S., Jia, Y., Yang, Y., Luo, L., Bi, A. and Fang, M., Bioinformatics Analyses of the Role of Vascular Endothelial Growth Factor in

Patients with Non-Small Cell Lung Cancer. *PLoS One*, 2015, **10**, e0139285.

13. Wang, S. W., Liu, S. C., Sun, H. L., Huang, T. Y., Chan, C. H., Yang, C. Y., Yeh, H. I., Huang, Y. L., Chou, W. Y. and Lin, Y. M., CCL5/CCR5 axis induces vascular endothelial growth factor-mediated tumor angiogenesis in human osteosarcoma microenvironment. *Carcinogenesis*, 2015, **36**, 104-114.

14. Pfister, N. T., Fomin, V., Regunath, K., Zhou, J. Y., Zhou, W., Silwalpandit, L., Freedpastor, W. A., Laptenko, O., Neo, S. P. and Bargonetti, J., Mutant p53 cooperates with the SWI/SNF chromatin remodeling complex to regulate VEGFR2 in breast cancer cells. *Genes & Development*, 2015, **29**, 1298-1315.

15. Smith, B. D., Kaufman, M. D., Leary, C. B., Turner, B. A., Wise, S. C., Ahn, Y. M., Booth, R. J., Caldwell, T. M., Ensinger, C. L. and Hood, M. M., Altiratinib Inhibits Tumor Growth, Invasion, Angiogenesis, and Microenvironment-Mediated Drug Resistance via Balanced Inhibition of MET, TIE2, and VEGFR2. *Molecular cancer therapeutics*, 2015, **14**.

16. Bainbridge, J. W. B., Jia, H., Bagherzadeh, A., Selwood, D., Ali, R. R. and Zachary, I., A peptide encoded by exon 6 of VEGF (EG3306) inhibits VEGF-induced angiogenesis in vitro and ischaemic retinal neovascularisation in vivo ☆. *Biochemical & Biophysical Research Communications*, 2003, **302**, 793-799.

17. Naganna, N. and Madhavan, N., Soluble non-cross-linked poly(norbornene) supports for peptide synthesis with minimal reagents. *Journal of Organic Chemistry*, 2014, **79**, 11549-11557.

18. Baxter, D., Ullman, C. G. and Mason, J. M., Library construction, selection and

modification strategies to generate therapeutic peptide-based modulators of protein-protein interactions. *Future Med. Chem*., 2014, **6**, 2073-2092.

19. Yang, Y., Zhou, J. and Yu, K., Design, synthesis, and in vitro evaluation of a binary targeting MRI contrast agent for imaging tumor cells. *Amino Acids*, 2014, **46**, 449-457.

20. Debergh, I., Damme, N. V., Naeyer, D. D., Smeets, P., Demetter, P., Robert, P., Carme, S., Pattyn, P. and Ceelen, W., Molecular Imaging of Tumor-Associated Angiogenesis Using a Novel Magnetic Resonance Imaging Contrast Agent Targeting α v β 3 Integrin. *Annals of Surgical Oncology*, 2014, **21**, 1-8.

21. Han, Z., Zhou, Z., Shi, X., Wang, J., Wu, X., Sun, D., Chen, Y., Zhu, H., Magi-Galluzzi, C. and Lu, Z.-R., EDB Fibronectin Specific Peptide for Prostate Cancer Targeting. *Bioconjugate chemistry*, 2015, **26**, 830-838.

22.LeungK.Antivascular endothelial growth factor polylactic acid-polyethylene glycol -poly-L-Lys/gadolinium-diethylenetriamine pentaacetic acid nanoparticles.Molecular Imaging and Contrast Agent Database (MICAD) [Internet]. Bethesda (MD): National Center for Biotechnology Information (US); 2004-2013.2012 May 05 [updated 2012 Jul 19].[PubMed: 22812022]

Figure Legends

Scheme 1. Illustration of proposed VGd binding to tumor extracellular matrix for MR signal enhancement

Figure 1. Chemical structures of VGd and SGd

Figure 2. MALDI-TOF spectra of VGd and SGd

Figure 3. The plots of $1/T_1$ and $1/T_2$ versus the concentration of VGd and SGd.

Figure 4. (a) In *vitro* MRI scans of BEL-7402 cells treated and untreated with SGd, VGd, and CPT, respectively. (b) The T1 signal-to-noise ratio (SNR) values of the samples treated and untreated with SGd, VGd, and CPT. $*p<0.01$ relative to others.

Figure 5. Immunohistochemical detection of VEGFR2 in tumor sections. (a) Hematoxylin-eosin staining showing large nuclei and (b) cell membranes positively stained for VEGFR2 for tumor sections used for treatment with VGd. (c) Hematoxylin-eosin staining and (d) cell membranes positively stained for VEGFR2 for tumor sections used for treatment with SGd. Green arrow indicated the VEGFR2 sites.

Figure 6. (a) T1-weighted MRI scans of tumor-bearing mice after tail vein injections of SGd or VGd. (b) Comparison of the T1 SNRs at various time points after the tail vein injections of SGd and VGd. $^{*}P < 0.01$ relative to SGd.

Figure 7. Biodistribution of gadolinium in the major organs and tissues of mice at day 1 and day 7 after administration of SGd and VGd at a dose of 0.2 mmol-Gd/kg in mice (n=5) bearing tumors. $*p < 0.01$ and $+p < 0.05$ relative to SGd.

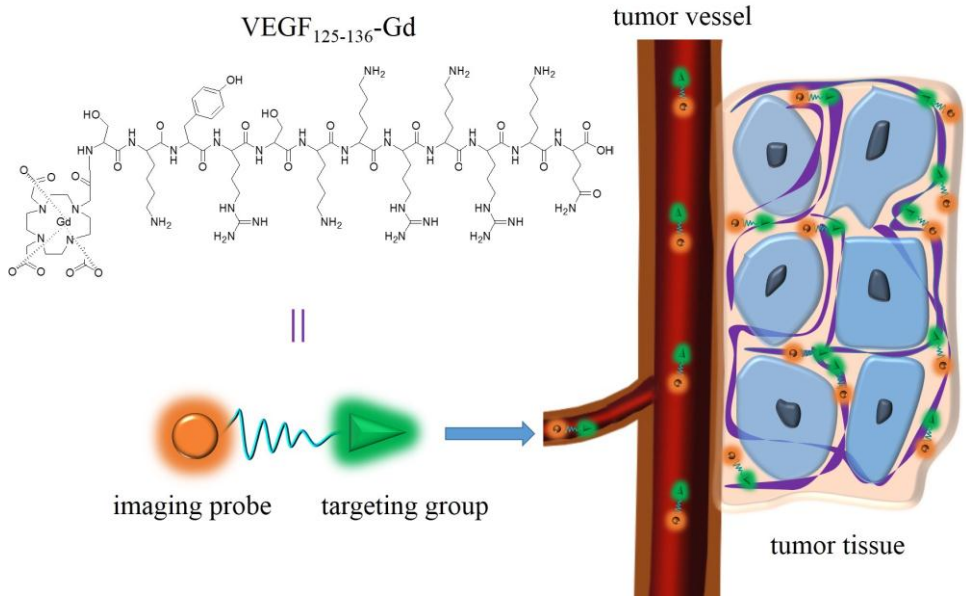

Scheme 1. Illustration of proposed VGd binding to BEL-7402 liver carcinoma cells for MR signal enhancement

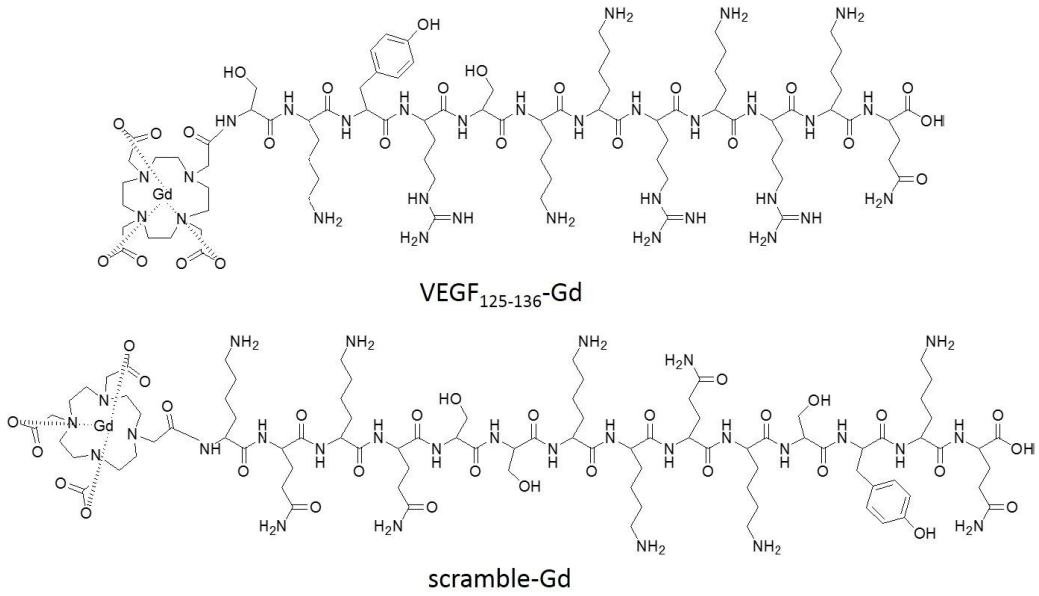

Figure 1. Chemical structures of VGd and SGd

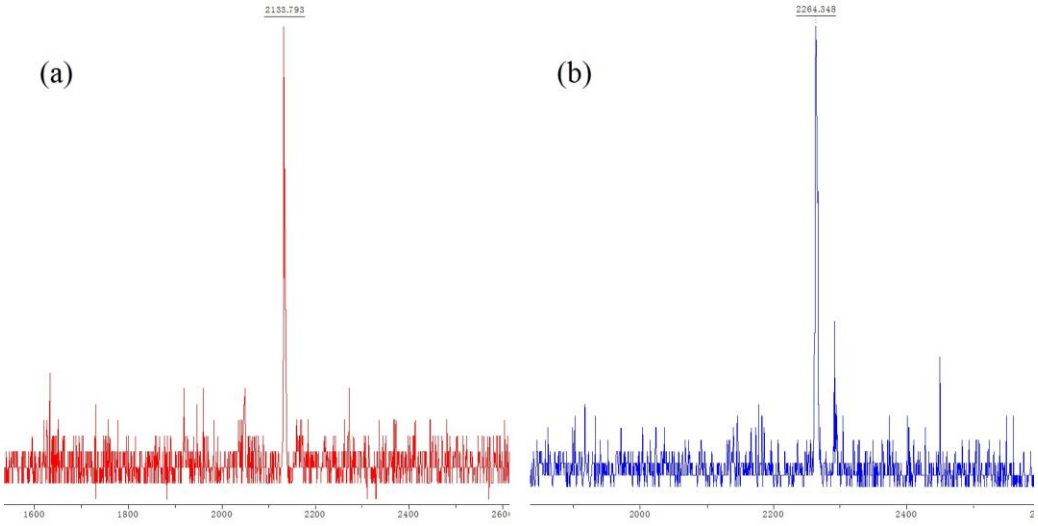

Figure 2. MALDI-TOF spectra of VGd and SGd

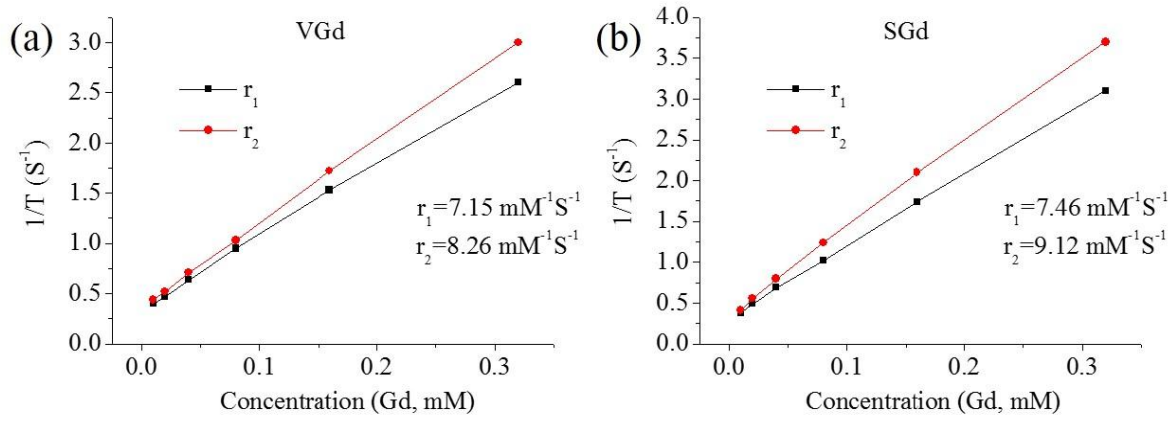

Figure 3. The plots of $1/T_1$ and $1/T_2$ versus the concentration of VGd and SGd.

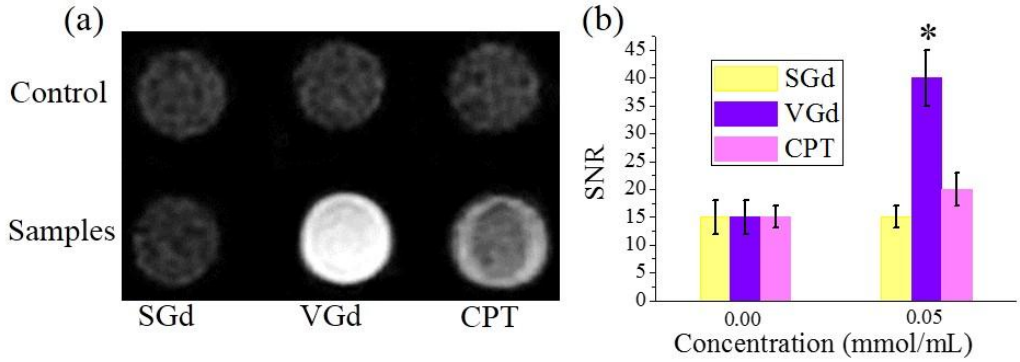

Figure 4. (a) In *vitro* MRI scans of BEL-7402 cells treated and untreated with SGd, VGd, and CPT, respectively. (b) The T1 signal-to-noise ratio (SNR) values of the samples treated and untreated with SGd, VGd, and CPT. *p<0.01 relative to others.

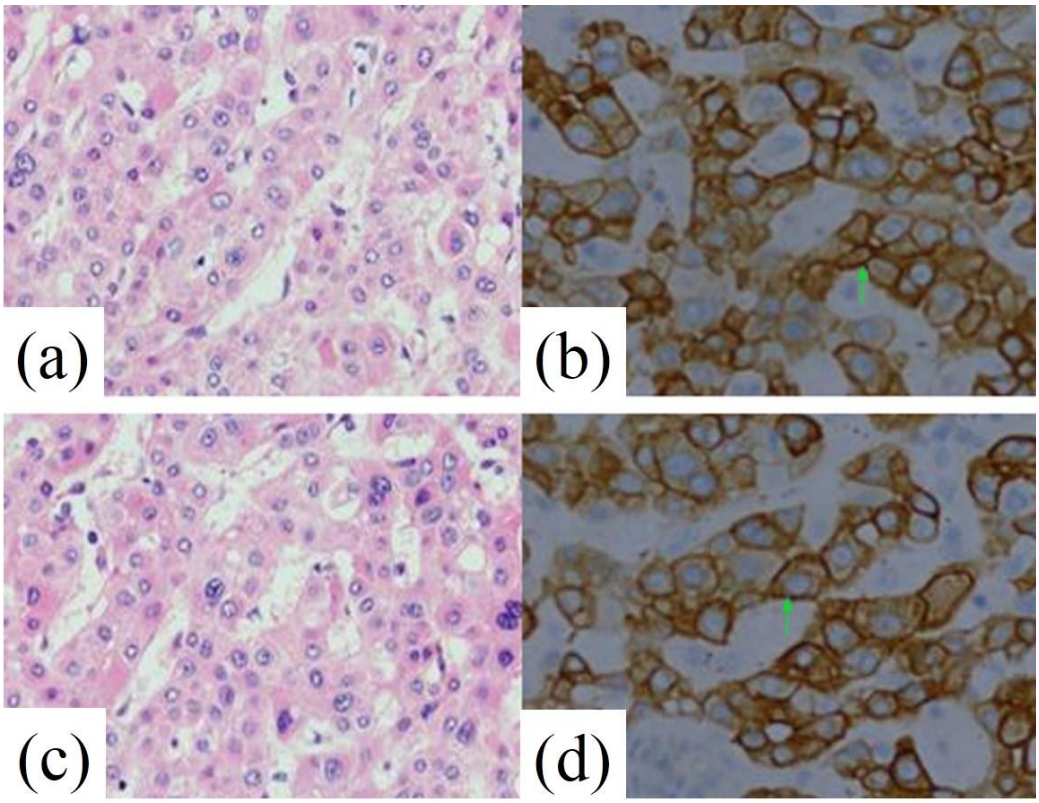

Figure 5. Immunohistochemical detection of VEGFR2 in tumor sections. (a) Hematoxylin-eosin staining showing large nuclei and (b) cell membranes positively stained for VEGFR2 for tumor sections used for treatment with VGd. (c) Hematoxylin-eosin staining and (d) cell membranes positively stained for VEGFR2 for tumor sections used for treatment with SGd. Green arrow indicated the VEGFR2 sites.

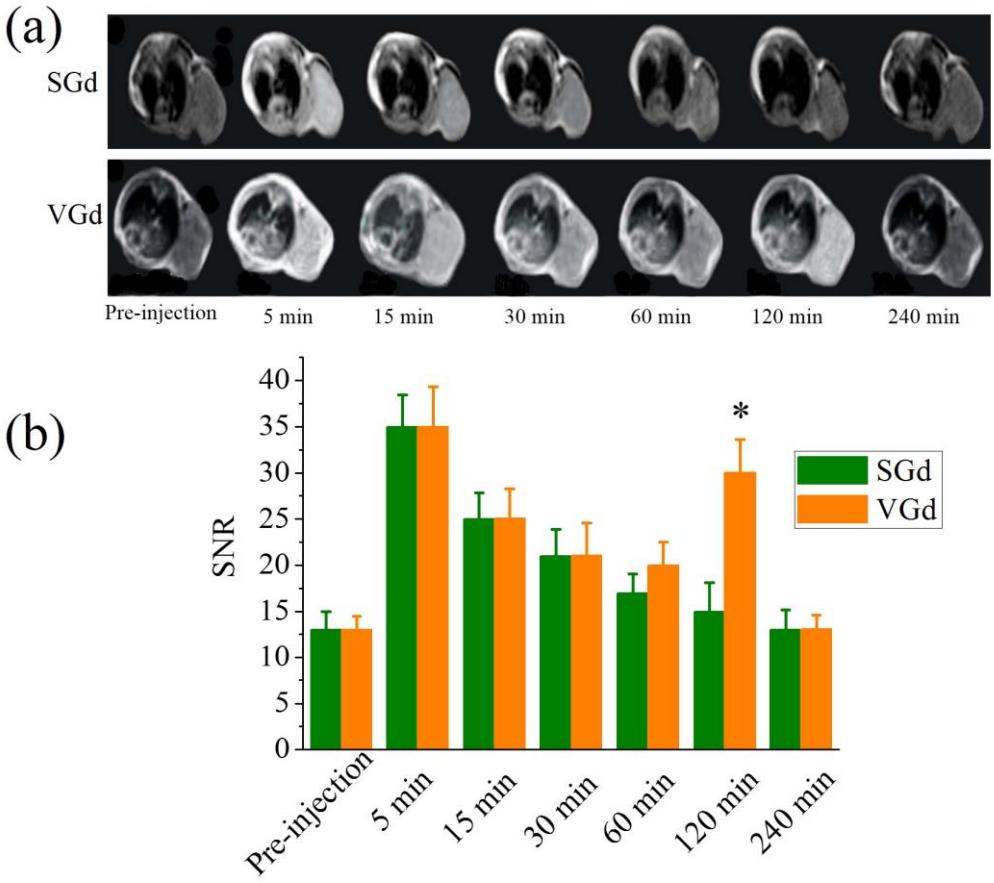

Figure 6. (a) T1-weighted MRI scans of tumor-bearing mice after tail vein injections of SGd or VGd. (b) Comparison of the T1 SNRs at various time points after the tail vein injections of SGd and VGd. $^{*}P < 0.01$ relative to SGd.

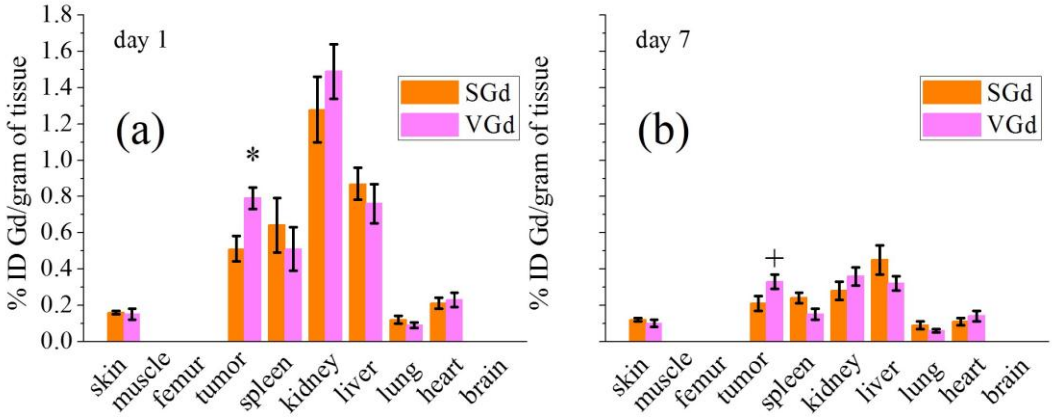

Figure 7. Biodistribution of gadolinium in the major organs and tissues of mice at day 1 and day 7 after administration of SGd and VGd at a dose of 0.2 mmol-Gd/kg in mice (n=5) bearing tumors. *$p < 0.01$ and +$p < 0.05$ relative to SGd.

A novel magnetic resonance imaging probe specifically targeting vascular endothelial growth factor receptor 2: synthesis, characterization, and biological evaluation

Xiaoguang You[a,b] and Yikai Xu[*,a]

[a]Department of Radiology, The Affiliated Hospital of Southern Medical University, Nanfang Hospital, No. 1838, Guangzhou Ave, Guangzhou, China

[b]Department of Radiology, The Affiliated Hospital of Hainan Medical University, No. 31, Longhua Road, Haikou,China

[*]Corresponding author: Yikai Xu, Department of Radiology, The Affiliated Hospital of Southern Medical University, Nanfang Hospital, No. 1838, Guangzhou Ave, Guangzhou, China

Telephone: +86 020-61642083; Email address: xyknfyy@126.com

Abstract: Vascular endothelial growth factor (VEGF) is strongly expressed in most tumors and promotes both tumor growth and vascularization. The peptide, $VEGF_{125-136}$, consisting of 12 amino acids is encoded by exon 6 of the *VEGF* gene and inhibits VEGF activity by blocking the binding of VEGF to the VEGFR2 receptor. The aim of the present study was to develop a targeting probe for magnetic resonance imaging (MRI) of tumors by conjugating $VEGF_{125-136}$ to gadolinium (III) (Gd(III)) (VGd) through the formation of chelates. The targeting efficiency of VGd to human hepatocellular carcinoma (HCC) cell line, BEL-7402, was subsequently determined both in *vitro* and in *vivo*. In the in *vitro* studies, the MRI results of BEL-7402 cells treated with VGd showed a significantly higher T1 signal-to-noise ratio than that of both the competitive group, namely, those treated with VGd and $VEGF_{125-136}$ and the control group, a scramble peptide conjugated to Gd(III) (SGd). In *vivo*, when xenografts of BEL-7402 cells were established in mice and then VGd or SGd were injected via tail vein, MRI showed that the tumor signal from VGd initially decreased from 5 min to 120 min and then it increased at 120 min post injection. The peak signal was observed at 120 min after the injection. In contrast, no distinct peak was observed for SGd. Undoubtedly, these findings indicate that VGd can target VEGFR2, highly expressed by BEL-7402 cells, enabling targeting MRI with high efficacy to be achieved both in *vitro* and in *vivo*.

Keywords:

$VEGF_{125-136}$; peptide; gadolinium; MRI; liver cancer xenograft

INTRODUCTION

Cancer is one of the most serious diseases that threaten human beings, and an early diagnosis of tumors, particularly for small ones, is of great importance for improving patient prognosis. Thus, an important task for molecular imaging is to generate accurate images that can facilitate the early diagnosis of cancers.[1] Most of the tumor-imaging agents currently used for MRI in the clinic are gadolinium Gd- or iron-based contrast agents, which generally image soft tissues with high spatial resolution and are effective for noninvasive imaging of physiological properties, such as diffusion, vascularity, and perfusion of the tissues of interest. However, the shortcoming of these agents limiting their broad application is the low sensitivity. The modification with targeting ligands, such as antibodies, proteins, and peptides, even though improved the probe delivery, it could not deliver a sufficient amount of agents to detect the target tissues.[2, 3] Thereby, nanoparticles have been used to load large amount of probes for increasing the local concentration of contrast agents.[2-4] The major limitation of nanoparticle-based MRI contrast agents is that they possess huger size than the renal filtration threshold (~4.5 nm), and cannot be readily excreted from the body, resulting in toxic side effects, for example, systemic nephrogenic fibrosis, particularly in case of long-term tissue retention of high-dose Gd(III)-based MRI agents.[5-9]

The challenges in MRI for molecular imaging can be overcome by the selection of molecular biomarkers and using MRI agents, which can be readily excreted from the

body. Stable Gd(III) chelates, such as DOTA, DO3A, DTPA, have been proven safe and receiving increasing attention as MRI agents.[2, 7, 10, 11] For targeted contrast agents, the sufficiently expressed biomarkers at local position play great role in molecular imaging. As previously reported, VEGF is strongly expressed in tumor tissues and its expression has been found to be proportional to the degree of malignancy for tumors.[12, 13] VEGF binds the VEGFR2 receptor which is also strongly expressed in most tumor cells, as well as in endothelial cells that mediate tumor neovascularization.[14, 15] Previously, $VEGF_{125\text{-}136}$, a 12-amino acid peptide encoded by exon 6 of the *VEGF* gene, was found to block the specific binding of VEGF to the VEGFR2 receptor.[16] Based on these findings, we hypothesized that targeted in *vivo* tumor imaging may be achieved with the use of Gd(III)-based contrast agents labeled with the $VEGF_{125\text{-}136}$ peptide as depicted in Scheme 1. Furthermore, the use of VGd as a contrast agent would provide a more widely applicable agent based on the strong expression profile of VEGF in many tumors. Therefore, in our present study, $VEGF_{125\text{-}136}$ will be conjugated to Gd(III) through the formation of chelates and its ability to target VEGFR2 in BEL-7402 liver carcinoma cells both in *vitro* and in *vivo* will be investigated. Our study might develop a promising Gd(III)-based targeted MRI agent with high imaging efficacy for potential clinical use.

MATERIALS AND METHODS

Materials

All chemicals and solvents were used without further purification unless otherwise stated. The Fmoc-protected $VEGF_{125\text{-}136}$ peptide (QKRKRKKSRYKS) resin and its

scrambled peptide (QKYSKQKKSSQKQK) resin were purchased from GL Biochem Ltd (China). 2-(1H-benzotriazol-1-yl)-1,1,3,3-tetramethyluronium hexafluorophosphate (HBTU), hydroxybenzotriazole (HOBt), and N,N-diisopropylethylamine (DIPEA) was purchased from Aladdin. Gadolinium acetic acid was purchased from Strem Chemicals (USA). Piperidine was purchased from Guangzhou Chemical Reagent Factory. DOTA-Tris (t-Bu ester) was purchased from TCL (Tokyo, Japan). Gadolinium acetic acid was obtained from Shanghai Di Bai Chemial Technology Co., Ltd.

General method of characterization

Matrix-assisted laser desorption/ionization time-of-flight (MALDI-TOF) mass spectra were recorded on a Bruker Autoflex III MALDI-TOF MS in a linear mode. T1 relaxation constants were measured with a 3.0T MRI scanner (GE, Pittsburgh, PA, USA) at 37 ℃ in distilled water. The Gd concentration in VGd or SGd was determined with an inductively coupled plasma mass spectrometer (ICP-MS, Thermo Fisher, USA).

Synthesis of Gd(III) chelates

The 12-amino acid $VEGF_{125-136}$ peptide (1.1 g) and the scrambled peptide (1.1 g) were deprotected with 15 ml piperidine/DMF solution (1:4, v/v) in solid phase peptide synthesis tubes to remove the Fmoc protecting groups. After washed with DMF (×3) and DCM (×3), DOTA-Tris (t-Bu ester) (290 mg, 0.5 mmol), HBTU (379 mg, 1 mmol), HOBt (100 mg), and DIPEA (500 μl) were added to each tube. The reaction continued under shaking at room temperature for 2 h. Then the resins were washed

with DMF (×3) and DCM (×3) before cleavage with a mixture of trifluoroacetic acid/triisobutylsilane/water (96.5:1.0:2.5, v/v/v) for 5 h. The products were subsequently precipitated with cold diethyl ether twice and dried under reduced pressure at room temperature to yield $VEGF_{125-136}$-DOTA or scramble-DOTA. MALDI-TOF ($VEGF_{125-136}$-DOTA) (*m*/*z*, $[M]^+$): 1978.36 (obsd.); 1978.15 (calcd). MALDI-TOF (scramble-DOTA) (*m*/*z*, $[M]^+$): 2109.43 (obsd.); 2109.15 (calcd).

The dried sample was further dissolved in 3 ml double-distilled water, to which gadolinium acetic acid (82 mg, 0.2 mmol) was added. During reaction, the pH was maintained at 6.5~7.0 at 50 ℃. After 24 h, the pH was adjusted to ~11 using aqueous NaOH (0.2 M) to remove most of the access Gd. Then the pH was neutralized to ~7 using HCl (0.2 M), followed by cold-drying to obtain crude white products. Further, the products was purified using high-performance liquid chromatography (HPLC), with a C18 column used for the stationary phase and acetonitrile/water applied for the mobile phase. MALDI-TOF (VGd) (*m*/*z*, $[M]^+$): 2133.79 (obsd.); 2133.06 (calcd). MALDI-TOF (SGd) (*m*/*z*, $[M]^+$): 2264.05 (obsd.); 2264.35 (calcd).

Cell culture

Human HCC cell line BEL-7402 (Chinese Academy of Medical Sciences, China) was grown in RPMI 1640 medium supplemented with 100 mL/L heat-inactivated fetal calf serum, 50,000 U/L penicillin, and 50 mg/L streptomycin. The cells were cultured under a humid condition (95%, relative humidity) at 37 ^oC containing 5% CO_2. The RPMI 1640 medium was refreshed every other day and the cells were split once the confluency was reached.

In *vitro* MRI examination

BEL-7402 cells were grown in RPMI 1640 medium in cell culture flasks (25 cm^3). When the cells reached 85% confluency, 100 μL of VGd (0.05 mmol/ml), 100 μL of SGd (0.05 mmol/ml), and 100 μL mixture of VGd and $VEGF_{125-136}$ as competitive probe test group (CPT, 0.05 mmol/ml, each) were added to flasks, respectively. Thereafter, the cells were incubated for 24 h at 37 ℃ under a humid condition at 5% CO_2. After the cells were washed with PBS (×4) and trypsinized, the cells were transferred to centrifuge tubes, followed by addition of 0.6% agarose to form a suspension. A 3.0-T MRI scanner head coil (GE, Pittsburgh, PA, USA) was used to obtain a MRI scan of each tube with the following T1 scanning parameters: repetition time (TR)/echo time (TE) = 600/15 ms, matrix = 256 × 256, thickness = 2 mm, field of view (FOV) = 20 cm, (signal-to-noise ratio = T1 mean signal/ambient noise), and region of interest (ROI) = 2 mm. The ROI was selected as the diameter for an effective T1 measuring range.

In *vivo* MR tumor imaging

Subaxillary xenografts of human BEL-7402 cells were established in 16 male nude mice (25-30 g, Slac Laboratory Animals Ltd., Shanghai, China). This animal study was approved by the independent Ethics Committee of Hainan Medical College Hospital, and all of the animals received humane care throughout the duration of the study. When the tumor diameter reached ~1.0 cm, the mice were anesthetized with pentobarbital (0.05 mg/g, i.p.) and administrated with of VGd (100 μL, 0.2 mmol

Gd/kg) and SGd (100 μL, 0.2 mmol Gd/kg) via tail vein injection. An additional 50 μL of saline was subsequently administered to flush the line and ensure that the complete dose was administered in each mouse. The mice then went through a MRI examination with a 3.0-T MRI scanner (GE) that had a dedicated mouse MRI coil (Chenguang Medical Technologies Ltd., Shanghai). Seven scans were performed on each mouse: the first scan was performed prior to the administration of contrast administration (pre-injection), while the followed scans were performed at 5, 15, 30, 60, 120, and 240 min post injection. All of the scans were conducted under the following axial fast-spin echo T1-weighted imaging conditions: TR/TE = 340/16 ms, number of excitations = 4, matrix = 128 × 128, FOV = 8 × 8 cm, slice thickness = 1.0 mm, and slice interval = 0.1. Signal intensity was obtained by averaging three measurements for three ROIs within the same slice at various time points. The diameter of each ROI was ~2.0 mm.

Immunohistological examination of VEGFR2 expression

For immunohistological staining of BEL-7402 xenografts, mice (n = 3) were injected with VGd or SGd. Then, the tumors were fixed with 4% formaldehyde, dehydrated in a gradient alcohol series and xylene, and embedded in paraffin. Sections (5 μm) were cut from each tissue block and mounted onto slides. After the sections were incubated overnight at 60 ℃, the sections were immersed in xylene (5 min×2) and then in a gradient alcohol series. After the sections were rinsed with water and 0.1 M PBS, they were immersed in methanol with 1% hydrogen peroxide at room temperature for 10

min before a final water rinse. The sections were subsequently treated with an antigen retrieval agent, rinsed with water, and blocked with non-immune horse serum. Subsequently, the sections were incubated with VEGFR2 antibody (Abcam) at 4 ℃ overnight and then washed with 0.1 M PBS, followed by incubation with an appropriate biotinylated secondary antibody (Abcam) for 20 min at 37 ℃. After rinsed with PBS, the sections were incubated with streptavidin-horseradish peroxidase at 37 ℃ for 20 min. After washed with PBS, bound antibodies were visualized with 3,3′-diaminobenzidine. A final thorough washing of the sections was followed by a counterstaining step with hematoxylin.

Biodistribution study

Tumor-bearing mice were sacrificed at 1 and 7 days post-injection. The tissues, for example, liver, lung, kidney, spleen, tumor, heart, brain, skin, femur, and muscle were collected. After dried and weighed, each sample was fully immersed in 70% nitric acid (1.0 mL). Once the sample was completely liquefied, the solution was transferred to a new centrifuge tube (15 mL) and the undissolved components were spinned down at 10,000 rpm for 20 min. Then the solution was filtrated through a syringe filter (0.22 μm, Nantong Feitebo membrane Co. Ltd, China) to further remove insoluble particles. Thereafter, the solution was diluted 10 times with deionized water and the Gd(III) concentration was detected by ICP. The average Gd(III) content in each tissue was calculated from the measured Gd(III) concentration and expressed as the percentage of injected dose per gram of organs (% ID/g).

RESULTS

The VGd and SGd in this study were purchased and used as received without further purification. After removal of the Fmoc protecting group, the free amine groups directly conjugate with DOTA-Tris (t-Bu ester) through solid-phase chemistry as shown in Figure 1. Thereafter, the products were cleaved from resins and formed chelates with gadolinium through carboxyl groups. The chemical structures of VGd and SGd were confirmed with MALDI-TOF spectra as demonstrated in Figure 2, which was also described in experimental section. The small peak appeared in the right of the major peak in Figure 2b should be ascribed to the addition of sodium element.

The plots of the T_1 and T_2 water proton relaxation values at 3.0T versus the concentration of VGd or SGd are demonstrated in Figure 3. The T1 relaxivity values (r_1) of VGd and SGd were measured to be 7.15 $mM^{-1}s^{-1}$ per Gd and 7.46 $mM^{-1}s^{-1}$ per Gd, respectively. Also, the T_2 relaxivity values (r_2) of them were determined to be 8.26 $mM^{-1}s^{-1}$ per Gd and 9.12 $mM^{-1}s^{-1}$ per Gd, respectively.

Figure 4 shows the results of the in *vitro* MRI examination of BEL-7402 cells treated with SGd, VGd and competitive group, respectively. Clearly, the samples, untreated with agents, showed extremely poor contrast. The similar result was also observed for the sample treated with SGd. Conversely, the sample treated with VGd presented significant contrast enhancement. In addition, even though the sample treated with CPT showed slightly improved contrast than the untreated groups, it was not comparable to the VGd-treated sample. Moreover, the T_1 signal-to-noise ratio (SNR) was measured accordingly at the concentrations of 0.00 and 0.05 mmol/mL as shown

in Figure 4b. Consistently, the VGd presented significantly higher SNR value than SGd and CPT groups.

To verify the targeting ability of VGd to VEGFR2 in *vivo*, it is paramount to confirm the availability of VEGFR2 in tumors. As shown in Figure 5, hematoxylin-eosin staining showed large nuclei with obvious isomerisms and visible mitotic figures and BEL-7402 tumor cell membranes positively displayed VEGFR2 for all tumor sections in the established xenografts of BEL-7402 cells. Hence, the tumors for VGd and SGd treatment in this study possessed the identical immunohistochemical conditions.

Further, the MRI scanning of tumor-bearing mice was performed to investigate the imaging effects of SGd and VGd as shown in Figure 6. The scanning time points were set at 5, 15, 30, 60, 120, and 240 min, respectively. Apparently, the images recorded from both agents reached the brightest point at 5 min and showed contrast decrease with time. However, compared with SGd, the VGd group presented relatively higher contrast enhancement at the same time point after 5 min and, moreover, it showed much slower contrast decrease. Interestingly, it showed great contrast enhancement at 120 min. Subsequently, the SNR values corresponding to the images were measured and plotted as depicted in Figure 6b, showing the consistent results.

To evaluate the retention of the contrast agents in the major organs, the biodistribution study was carried out at day 1 and day 7 post-injection in the tumor-bearing mice. The major organs were dissolved in high purity nitric acid and the Gd(III) content was measured by ICP. Figure 7 showed the biodistribution of SGd or VGd in the major organs, including muscle, femur, tumor, skin, spleen, liver, kidney, lung, heart, and

brain at day 1 and day 7 post-injection at a dose of 0.2 mmol-Gd/kg. The retention of SGd and VGd was comparable in the normal tissues and was significantly different ($p<0.01$) in the tumor at day 1 post-injection. At day 7, the retention of VGd in tumor was still significantly higher than SGd ($p<0.05$).

DISCUSSION

Development of targeted MRI molecular probes is of great importance in molecular imaging since it has the potential to improve tumor visualization and positioning accuracy. Generally, the imaging component of probes includes iron- or gadolinium-based contrast agents, while the targeting ligands popularly studied are antibodies, peptides, and aptamers. Peptides are particularly advantageous because of their low molecular weight, ease of transportation and storage, great stability, and ease of modification.[17, 18] For example, recent studies have demonstrated that the use of $\alpha_v\beta_3$ integrin, aminopeptidase N, and angiopoietin could provide targeting of a tumor and its vascular endothelial cells.[19, 20]

VEGF has 7 exon sequences, and the affinity of the peptide fragments encoded by these exons for VEGFR2 varies considerably. Previous findings suggested that the affinity of $VEGF_{125\text{-}136}$ (QKRKRKKSRYKS), a 12-amino acid peptide encoded by exon 6 for VEGFR2, was greater than that of other similar peptide fragments.[16] Furthermore, binding of $VEGF_{125\text{-}136}$ to the extracellular region of VEGFR2 has no biological activity, yet this binding event can competitively prevent the ability of VEGF from promoting tumor cell growth and angiogenesis. Therefore, irreversibly

linking $VEGF_{125-136}$ with Gd via chemical bonds was expected to provide a targeted MRI imaging enhancement.

In our present study, we first synthesized VGd and SGd through a facile standard solid-phase chemistry as demonstrated in Figure 1. MALDI-TOF (Figure 2) was employed to confirm the molecular weights of VGd and SGd (2133.52 g/mol and 2264.60 g/mol, respectively), and these weights matched their theoretical molecular weights, meaning that the chemical structures shown in Figure 1 were obtained. Furthermore, the relaxivity values including r_1 and r_2 at 3.0T for both SGd and VGd were confirmed as shown in Figure 3. The results indicated that both r_1 and r_2 of SGd were slightly higher than those of VGd. Earlier study on the MRI contrasts using CREKA as targeting peptide demonstrated that its r_1 and r_2 values were also slightly lower than those of the scrambled peptide.[11] However, the essential point in this study is to demonstrate the advantageous targeting ability of VGd over SGd. Therefore, the targeting effect will be valued more than the relaxivity, not to mention the slight difference between VGd and SGd. This question was further elucidated in the in *vitro* imaging study as indicated in Figure 4. In principle, the SGd with higher r_1 value was expected to show enhanced contrast compared with VGd since MRI agents with higher relaxivity would provide equivalent contrast at a lower dose compared with lower relaxivity agents.[7, 11] However, the results suggested that the VGd with slightly lower r_1 gave significantly greater imaging enhancement than SGd at the concentration of 0.05 mmol/mL than SGd, indicating that the targeting effect from $VEGF_{125-136}$ dominated the interaction of agents with cells. To further confirm the targeting efficacy of VGd to cells, the competitive group was added and the cells showed much poorer imaging contrast than VGd, which might attribute to the competitive binding of $VEGF_{125-136}$ to VEGFR2. These imaging studies and the

quantified SNR values in Figure 4b consistently demonstrated the great targeting efficacy of VGd to tumor cells.

To ensure the existence of VEGFR2 in tumors for both VGd and SGd groups, positive immunohistochemical staining of BEL-7402 cell membranes for VEGFR2 was employed for confirmation as shown in Figure 5, indicating the same tumor condition for both VGd and SGd groups. Further, tail vein injections of VGd or SGd were conducted to evaluate the in *vivo* imaging of contrast agents. It is found that efficient accumulation of the targeted contrast agent was observed in the tumor area at 5 min, however the contrast continuously decreased faster after 5 min for SGd than VGd. Previously, the other peptides used for MRI targeting imaging, including CREKA, ZD2, and CLT1, also indicated the similar findings that agents modified with targeting peptides would provide enhanced contrast and also slower contrast decrease with scanning time.[2, 11, 21] As illustrated in Scheme 1, the VGd, once injected via tail vein, circulated in the blood vessel and conveniently bound to the VEGFR2 highly expressed in tumors, resulting in the improved tumor uptake of VGd compared with SGd. On the contrary, SGd without targeting funtion can be easily eliminated from the mouse body within short time post-injection, certainly strongly lowering its imaging efficacy. In addition, we noted that the contrast was sharply enhanced at 120 min for VGd. Previously, Gd-labeled VEGF monoclonal antibodies was injected via a caudal intravenous injection into a mouse model of a hepatocellulcar carcinoma (HCC) hepatic transplantable tumor, the contrast agent was detected at 10 min post-injection.[22] More interestingly, the highest contrast enhancement was detected at 120 min and then the signal disappeared completely within 24 h. These results are similar to those of the present study, except that the signal for the contrast reagent was maintained for a longer period than that in the present study. It is possible that the

larger molecular weight of the monoclonal VEGF antibodies in that study underwent longer circulation time.

The retention of both agents was comparable in the normal tissues and the VGd accumulation was significantly higher in the tumor post-injection as shown in Figure 7. The targeted contrast agent displayed higher tumor uptake than the non-targeted contrast agent. The injected agents were, mostly, eliminated from the mouse within short period. The kidneys and liver, the major organ involved in the excretion of contrast agents, had a Gd(III) retention of the injected VGd or SGd per gram of tissue, higher than other organs and tissues.[11] At day 7, the Gd(III) retention was remakablly decreased in the kidneys and liver. No detectable Gd(III) was observed in the bone, muscle or brain for SGd or VGd, indicating that our contrast agent should have great safety for potential clinical use. As compared with previously reported dendrimer-based targeted Gd(III) chelates, the peptide targeted low molecular weight contrast agent, VGd, has much lower Gd(III) retention in *vivo*.

Summary

An amide linkage was used to conjugate $VEGF_{125-136}$ to Gd to develop a novel targeted contrast agent that has high T1 relaxivity. In BEL-7402 tumor cells, $VEGF_{125-136}$-Gd was found to effectively target VEGFR2 both *in vitro* and *in vivo*, and thus, this agent may be useful for targeted MRI imaging.

Acknowledgments

We would like to thank Zheng-Rong Lu (Department of Biomedical Engineering,

Case Western Reserve University, Cleveland, OH) for his guidance in the probe construction efforts. This study was funded by the National Natural Science Foundation of China (Grant no. 81160177, 81641067 and 81460262) and the Natural Science Foundation of Hainan, China (Grant no. 20158290).

Conflict of Interest

The authors declare no conflict of interest.

References

1. Li, C., Chen, T., Ocsoy, I., Zhu, G., Yasun, E., You, M., Wu, C., Zheng, J., Song, E., Huang, C. Z. and Tan, W., Gold-Coated Fe3O4 Nanoroses with Five Unique Functions for Cancer Cell Targeting, Imaging, and Therapy. *Advanced Functional Materials*, 2014, **24**, 1772-1780.

2. Tan, M., Ye, Z., Lindner, D., Brady-Kalnay, S. M. and Lu, Z. R., Synthesis and evaluation of a targeted nanoglobular dual-modal imaging agent for MR imaging and image-guided surgery of prostate cancer. *Pharm. Res.*, 2014, **31**, 1469-1476.

3. Li, J., Huang, S., Shao, K., Liu, Y., An, S., Kuang, Y., Guo, Y., Ma, H., Wang, X. and Jiang, C., A choline derivate-modified nanoprobe for glioma diagnosis using MRI. *Scientific Reports*, 2013, **3**, 1623.

4. Kuo, T., Lai, W., Li, C., Wun, Y., Chang, H., Chen, J., Yang, P. and Chen, C., AS1411 aptamer-conjugated Gd2O3:Eu nanoparticles for target-specific computed tomography/magnetic resonance/fluorescence molecular imaging. *Nano Research*, 2014, **7**, 658-669.

5. Curtet, C., Maton, F., Havet, T., Slinkin, M., Mishra, A., Chatal, J. F. and Muller, R. N., Polylysine-Gd-DTPAn and polylysine-Gd-DOTAn coupled to anti-CEA F(ab')2 fragments as potential immunocontrast agents. Relaxometry, biodistribution, and magnetic resonance imaging in nude mice grafted with human colorectal carcinoma. *Investigative radiology*, 1998, **33**, 752-761.

6. Ke, T., Jeong, E. K., Wang, X., Feng, Y., Parker, D. L. and Lu, Z. R., RGD targeted poly(L-glutamic acid)-cystamine-(Gd-DO3A) conjugate for detecting

angiogenesis biomarker alpha(v) beta3 integrin with MRT, mapping. *Int. J. Nanomed.* 2007, **2**, 191-199.

7. Flacke, S., Fischer, S., Scott, M. J., Fuhrhop, R. J., Allen, J. S., Mclean, M., Winter, P., Sicard, G. A., Gaffney, P. J. and Wickline, S. A., Novel MRI Contrast Agent for Molecular Imaging of Fibrin Implications for Detecting Vulnerable Plaques. *Circulation* 2001, **104**, 1280-1285.

8. Amirbekian, V., Lipinski, M. J., Briley-Saebo, K. C., Amirbekian, S., Aguinaldo, J. G. S., Weinreb, D. B., Vucic, E., Frias, J. C., Hyafil, F. and Mani, V., Detecting and assessing macrophages in vivo to evaluate atherosclerosis noninvasively using molecular MRI. *Proceedings of the National Academy of Sciences of the United States of America,* 2007, **104**, 961-966.

9. Sieber, M. A., Pietsch, H., Walter, J., Haider, W., Frenzel, T. and Weinmann, H. J., A preclinical study to investigate the development of nephrogenic systemic fibrosis: a possible role for gadolinium-based contrast media. *Investigative radiology*, 2008, **43**, 65-75.

10. Tan, M. and Lu, Z. R., Integrin Targeted MR Imaging. *Theranostics* 2011, **1**, 83-101.

11. Zhou, Z., Wu, X., Kresak, A., Griswold, M. and Lu, Z.-R., Peptide targeted tripod macrocyclic Gd(III) chelates for cancer molecular MRI. *Biomaterials*, 2013, **34**, 7683-7693.

12. Wang, Y., Huang, L., Wu, S., Jia, Y., Yang, Y., Luo, L., Bi, A. and Fang, M., Bioinformatics Analyses of the Role of Vascular Endothelial Growth Factor in

Patients with Non-Small Cell Lung Cancer. *PLoS One*, 2015, **10**, e0139285.

13. Wang, S. W., Liu, S. C., Sun, H. L., Huang, T. Y., Chan, C. H., Yang, C. Y., Yeh, H. I., Huang, Y. L., Chou, W. Y. and Lin, Y. M., CCL5/CCR5 axis induces vascular endothelial growth factor-mediated tumor angiogenesis in human osteosarcoma microenvironment. *Carcinogenesis*, 2015, **36**, 104-114.

14. Pfister, N. T., Fomin, V., Regunath, K., Zhou, J. Y., Zhou, W., Silwalpandit, L., Freedpastor, W. A., Laptenko, O., Neo, S. P. and Bargonetti, J., Mutant p53 cooperates with the SWI/SNF chromatin remodeling complex to regulate VEGFR2 in breast cancer cells. *Genes & Development*, 2015, **29**, 1298-1315.

15. Smith, B. D., Kaufman, M. D., Leary, C. B., Turner, B. A., Wise, S. C., Ahn, Y. M., Booth, R. J., Caldwell, T. M., Ensinger, C. L. and Hood, M. M., Altiratinib Inhibits Tumor Growth, Invasion, Angiogenesis, and Microenvironment-Mediated Drug Resistance via Balanced Inhibition of MET, TIE2, and VEGFR2. *Molecular cancer therapeutics*, 2015, **14**.

16. Bainbridge, J. W. B., Jia, H., Bagherzadeh, A., Selwood, D., Ali, R. R. and Zachary, I., A peptide encoded by exon 6 of VEGF (EG3306) inhibits VEGF-induced angiogenesis in vitro and ischaemic retinal neovascularisation in vivo ☆. *Biochemical & Biophysical Research Communications*, 2003, **302**, 793-799.

17. Naganna, N. and Madhavan, N., Soluble non-cross-linked poly(norbornene) supports for peptide synthesis with minimal reagents. *Journal of Organic Chemistry*, 2014, **79**, 11549-11557.

18. Baxter, D., Ullman, C. G. and Mason, J. M., Library construction, selection and

modification strategies to generate therapeutic peptide-based modulators of protein-protein interactions. *Future Med. Chem*., 2014, **6**, 2073-2092.

19. Yang, Y., Zhou, J. and Yu, K., Design, synthesis, and in vitro evaluation of a binary targeting MRI contrast agent for imaging tumor cells. *Amino Acids*, 2014, **46**, 449-457.

20. Debergh, I., Damme, N. V., Naeyer, D. D., Smeets, P., Demetter, P., Robert, P., Carme, S., Pattyn, P. and Ceelen, W., Molecular Imaging of Tumor-Associated Angiogenesis Using a Novel Magnetic Resonance Imaging Contrast Agent Targeting α v β 3 Integrin. *Annals of Surgical Oncology*, 2014, **21**, 1-8.

21. Han, Z., Zhou, Z., Shi, X., Wang, J., Wu, X., Sun, D., Chen, Y., Zhu, H., Magi-Galluzzi, C. and Lu, Z.-R., EDB Fibronectin Specific Peptide for Prostate Cancer Targeting. *Bioconjugate chemistry*, 2015, **26**, 830-838.

22.LeungK.Antivascular endothelial growth factor polylactic acid-polyethylene glycol -poly-L-Lys/gadolinium-diethylenetriamine pentaacetic acid nanoparticles.Molecular Imaging and Contrast Agent Database (MICAD) [Internet]. Bethesda (MD): National Center for Biotechnology Information (US); 2004-2013.2012 May 05 [updated 2012 Jul 19].[PubMed: 22812022]

Figure Legends

Scheme 1. Illustration of proposed VGd binding to tumor extracellular matrix for MR signal enhancement

Figure 1. Chemical structures of VGd and SGd

Figure 2. MALDI-TOF spectra of VGd and SGd

Figure 3. The plots of $1/T_1$ and $1/T_2$ versus the concentration of VGd and SGd.

Figure 4. (a) In *vitro* MRI scans of BEL-7402 cells treated and untreated with SGd, VGd, and CPT, respectively. (b) The T1 signal-to-noise ratio (SNR) values of the samples treated and untreated with SGd, VGd, and CPT. $*p<0.01$ relative to others.

Figure 5. Immunohistochemical detection of VEGFR2 in tumor sections. (a) Hematoxylin-eosin staining showing large nuclei and (b) cell membranes positively stained for VEGFR2 for tumor sections used for treatment with VGd. (c) Hematoxylin-eosin staining and (d) cell membranes positively stained for VEGFR2 for tumor sections used for treatment with SGd. Green arrow indicated the VEGFR2 sites.

Figure 6. (a) T1-weighted MRI scans of tumor-bearing mice after tail vein injections of SGd or VGd. (b) Comparison of the T1 SNRs at various time points after the tail vein injections of SGd and VGd. $^{*}P < 0.01$ relative to SGd.

Figure 7. Biodistribution of gadolinium in the major organs and tissues of mice at day 1 and day 7 after administration of SGd and VGd at a dose of 0.2 mmol-Gd/kg in mice (n=5) bearing tumors. $*p < 0.01$ and $+p < 0.05$ relative to SGd.

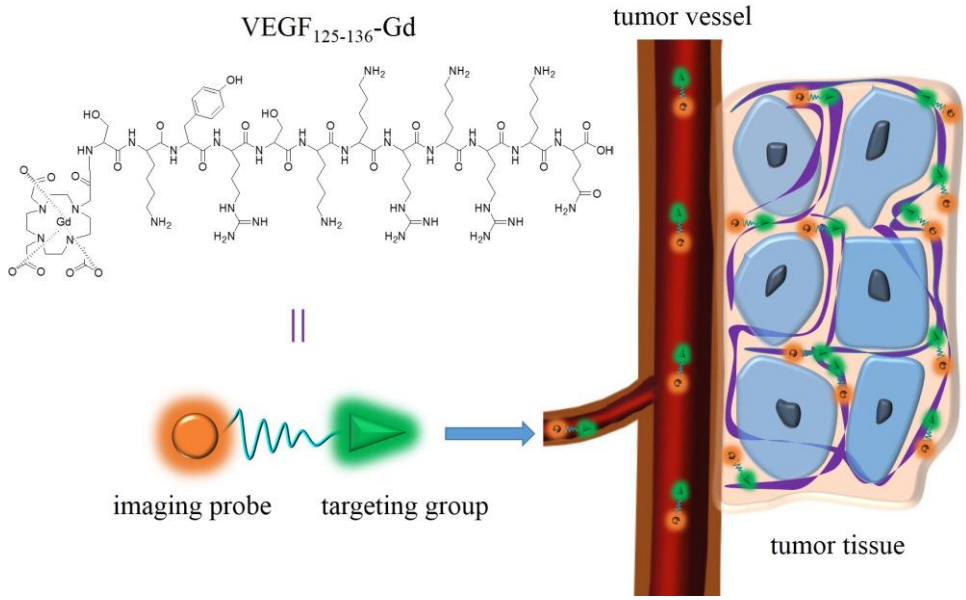

Scheme 1. Illustration of proposed VGd binding to BEL-7402 liver carcinoma cells for MR signal enhancement

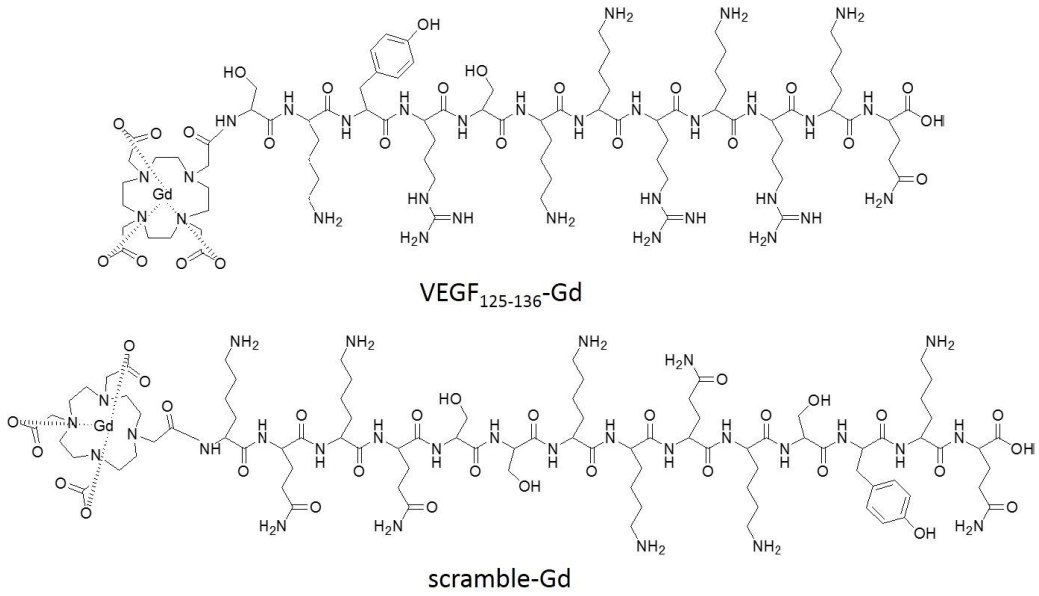

Figure 1. Chemical structures of VGd and SGd

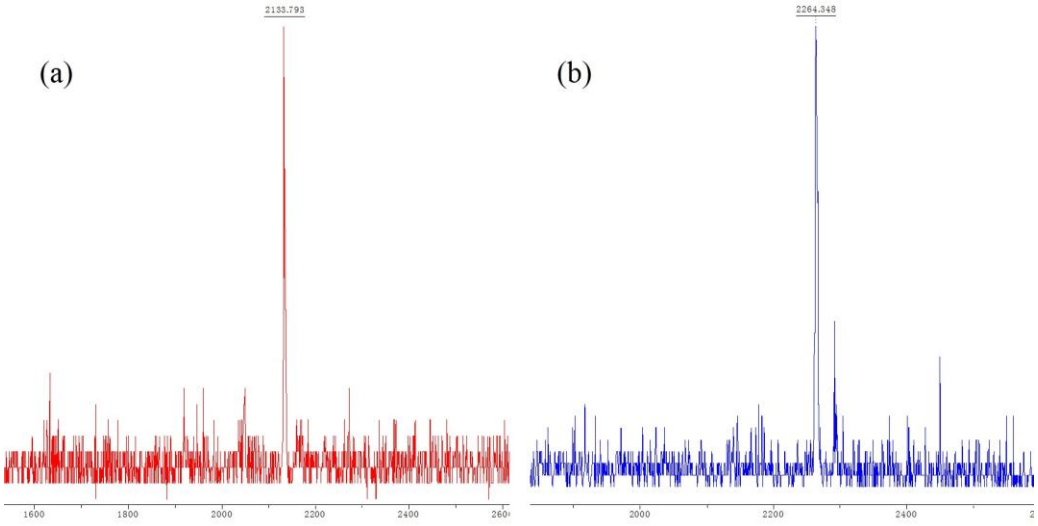

Figure 2. MALDI-TOF spectra of VGd and SGd

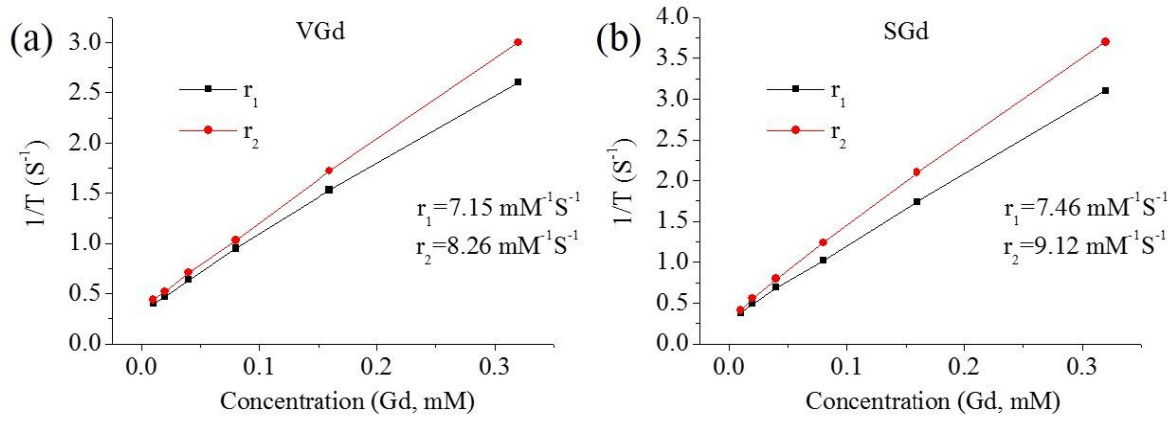

Figure 3. The plots of $1/T_1$ and $1/T_2$ versus the concentration of VGd and SGd.

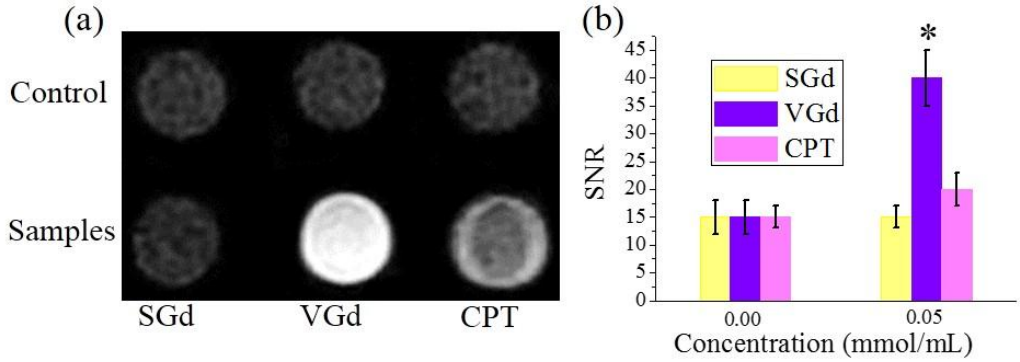

Figure 4. (a) In *vitro* MRI scans of BEL-7402 cells treated and untreated with SGd, VGd, and CPT, respectively. (b) The T1 signal-to-noise ratio (SNR) values of the samples treated and untreated with SGd, VGd, and CPT. *p<0.01 relative to others.

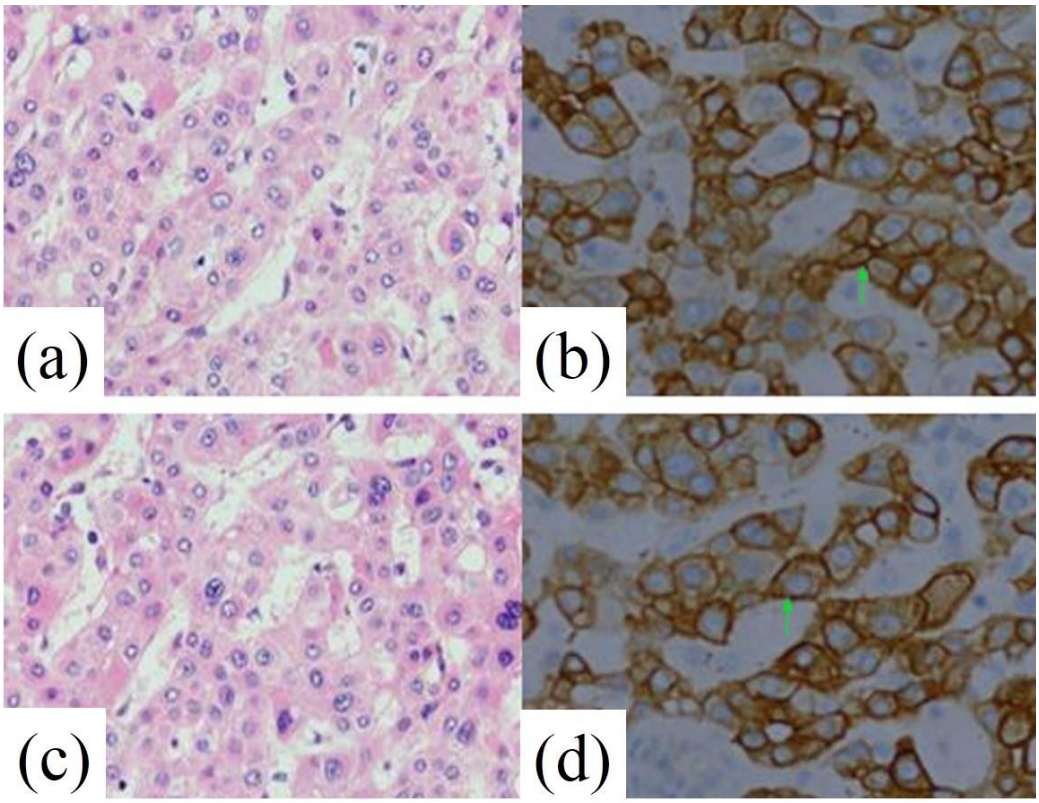

Figure 5. Immunohistochemical detection of VEGFR2 in tumor sections. (a) Hematoxylin-eosin staining showing large nuclei and (b) cell membranes positively stained for VEGFR2 for tumor sections used for treatment with VGd. (c) Hematoxylin-eosin staining and (d) cell membranes positively stained for VEGFR2 for tumor sections used for treatment with SGd. Green arrow indicated the VEGFR2 sites.

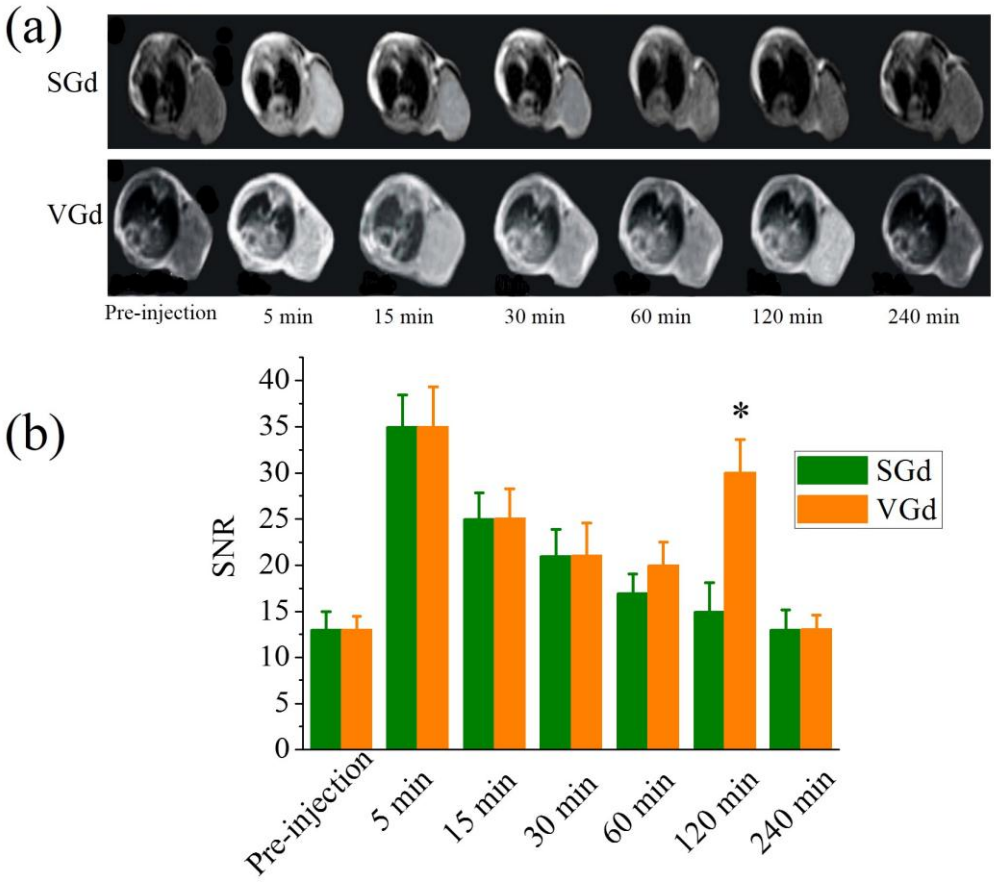

Figure 6. (a) T1-weighted MRI scans of tumor-bearing mice after tail vein injections of SGd or VGd. (b) Comparison of the T1 SNRs at various time points after the tail vein injections of SGd and VGd. $^{*}P < 0.01$ relative to SGd.

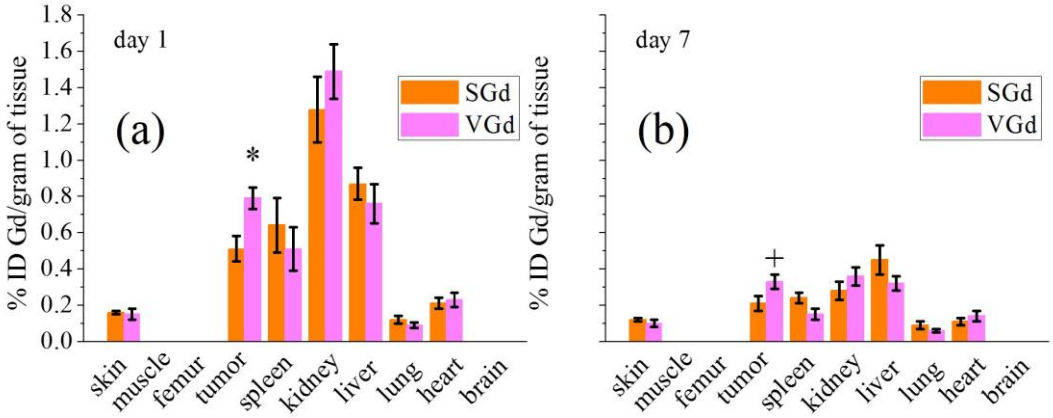

Figure 7. Biodistribution of gadolinium in the major organs and tissues of mice at day 1 and day 7 after administration of SGd and VGd at a dose of 0.2 mmol-Gd/kg in mice (n=5) bearing tumors. *$p < 0.01$ and +$p < 0.05$ relative to SGd.